

indeed occurs — can be traced through the measurements of the coupling constants changes in course of cosmic time (e.g., Avelino et al. 2006). Theories predict different behavior of dark energy, from slow-rolling to oscillating (e.g., Liddle & Lyth 2000; Fujii & Maeda 2003). It is clear that in order to study the dynamics of dark energy the fundamental constants must be measured at every redshift z with highest accuracy.

The value of $\Delta\alpha/\alpha = (\alpha_z - \alpha)/\alpha$ at a redshift z can be estimated from the radial velocity shifts of the line positions of different ions. Theoretical basics of the method called ‘Many Multiplet (MM) method’ are given in Webb et al. (1999) and Dzuba et al. (2002). Recently obtained results are as follows.

Murphy et al. (2004) claim that $\Delta\alpha/\alpha = -5.7 \pm 1.1$ ppm (ppm stands for parts per million, 10^{-6}) in the redshift range $0.2 < z < 4.2$, i.e. α was lower in the past. This result was produced by averaging over 143 absorption systems detected in HIRES/Keck telescope spectra of QSOs. However, Chand et al. (2004) report $\Delta\alpha/\alpha = -0.6 \pm 0.6$ ppm for $0.4 < z < 2.3$ from the analysis of 23 absorption systems identified in the UVES/VLT spectra of QSOs. It should be emphasized that

- both the Murphy et al. and Chand et al. estimates are obtained by averaging over many absorption systems with different redshifts, i.e. the accuracy of $\Delta\alpha/\alpha$ at individual redshifts is considerably lower than the reported values;
- Mg II and Fe II ions — the main elements of the most accurate low- z sample by Murphy et al. — cannot be formed in the same volume of the intervening metal absorbers as shown from spectral observations of GRBs (Hao et al. 2006; Porciani et al. 2007).

Recent laboratory restriction on the rate of fractional variation of the fine-structure constant of $(-2.7 \pm 2.6) \times 10^{-15} \text{ yr}^{-1}$ (Cingöz et al. 2007), which is based on highly sensitive to temporal variation of α transition frequencies in two isotopes of dysprosium (Dy), indicates no significant variation at present time ($z = 0$). Revision of the fission products of a natural reactor in Oklo ($z = 0.4$) also indicates no variation at the level of $1.2 \times 10^{-17} \text{ yr}^{-1}$ (Gould et al. 2006).

In order to improve the accuracy of individual $\Delta\alpha/\alpha$ values measured from quasar absorption-line spectra, we developed a modification of the MM method called ‘Single Ion Differential α Measurement, SIDAM’ (Levshakov 2004; Quast et al. 2004; Levshakov et al. 2005, hereafter Paper I; Levshakov et al. 2006, hereafter Paper II). Based on the analysis of only one element (singly charged iron, Fe II), it is free from the influence of small Doppler shifts between different elements caused by ionization inhomogeneities within the absorber, and by unknown isotopic abundances. It is also free from different

line profile distortions due to finite correlation length effects in turbulent velocity fields which are sensitive to the ratio of the rms turbulent velocity to the thermal width of the absorbing ions (Levshakov & Kegel 1997; Levshakov et al. 1997).

Using SIDAM, we have reached the accuracy of $\Delta\alpha/\alpha$ for one absorption system at the level of $\sim 10^{-6}$, i.e. as high as the accuracy of the mentioned above values averaged over many absorption systems. Our previous results give the following constraints on $\Delta\alpha/\alpha$.

At $z_{\text{abs}} = 1.15$ towards HE 0515-4414, $\Delta\alpha/\alpha = -0.4 \pm 1.9$ ppm at $z_{\text{abs}} = 1.15$ (Quast et al. 2004). Later on, we improved the accuracy of this estimation and obtained $\Delta\alpha/\alpha = -0.07 \pm 0.84$ ppm (Paper II). This utmost accuracy was achieved due to unique favorable conditions such as the brightness of the quasar and the strength of all Fe II lines including $\lambda 1608 \text{ \AA}$. In both cases the same archive data were used: $FWHM \simeq 5.6 \text{ km s}^{-1}$ in the blue and $\simeq 4.8 - 5.5 \text{ km s}^{-1}$ in the red. A consistent restriction on $\Delta\alpha/\alpha$ in this system was obtained independently by Chand et al. (2006), $\Delta\alpha/\alpha = 0.5 \pm 2.4$ ppm, who used the high resolution pressure and temperature stabilized spectrograph HARPS mounted on the ESO 3.6 m telescope at the La Silla observatory.

Further, using the VLT/UVES archive spectra of Q 1101-264 with the resolution $FWHM \simeq 6.0 \text{ km s}^{-1}$ in the blue ($\lambda \sim 4500 \text{ \AA}$), and $\simeq 5.4 \text{ km s}^{-1}$ in the red ($\lambda \sim 7000 \text{ \AA}$) we obtained $\Delta\alpha/\alpha = 2.4 \pm 3.8$ ppm at $z_{\text{abs}} = 1.839$ (Paper I).

Recently this quasar was re-observed with higher spectral resolution. In the present paper we describe the new measurement of $\Delta\alpha/\alpha$ at $z_{\text{abs}} = 1.839$ which allowed us to enhance the accuracy of $\Delta\alpha/\alpha$ by a factor 1.5.

2. Observations and Data Reduction

The observations of Q 1101-264 were acquired with the VLT UV-Visual Echelle Spectrograph (UVES) on the nights of 2006 February 21, 22, and 23. The selected exposures are listed in Table 1. The spectra were recorded with a dichroic filter which allows to work with the blue and red UVES arms simultaneously as with two independent spectrographs, and the CCDs were read out unbinned. The standard settings at central wavelengths $\lambda 437 \text{ nm}$ and $\lambda 860 \text{ nm}$ were used for the blue and red arms respectively (marked by symbols ‘b’ and ‘r’ in Col. 1 of Table 1). The slit was oriented along the parallactic angle and the width set at 0.5 arcsec , with DIMM values ranging from 0.5 to 1.1 arcsec during the run.

Calibration exposures were taken immediately after scientific exposures to minimize the influence of changing ambient weather conditions which may cause different velocity offsets in the lamp and QSO spectra if they were not obtained closely in time (Paper II). Variations in tem-

Table 1. UVES/VLT observations of Q 1101–264 (ESO programme 076.A-0463)

Exp. No. (1)	Date y-m-d (2)	Time h:m:s (3)	Exp. s (4)	S/N per pixel (5)
1b	2006-02-21	07:39:26	6400	30
1r	2006-02-21	07:39:22	5400	32,34
2b	2006-02-22	02:28:57	5400	31
2r	2006-02-22	02:28:52	5400	39,37
3b	2006-02-22	04:04:47	4953	30
3r	2006-02-22	04:04:43	4959	44,44
4b	2006-02-22	05:55:21	5400	34
4r	2006-02-22	05:55:17	5400	47,49
5b	2006-02-22	07:30:28	6708	38
5r	2006-02-22	07:30:25	6712	52,48
6b	2006-02-23	01:29:26	6300	26
6r	2006-02-23	01:29:25	6300	36,38
7b	2006-02-23	03:19:23	7200	35
7r	2006-02-23	03:19:22	7200	46,48
8b	2006-02-23	05:45:15	5400	37
8r	2006-02-23	05:45:10	5400	41,46
9b	2006-02-23	07:19:40	7500	40
9r	2006-02-23	07:19:34	7500	52,53

Note: in Col. 1, ‘b’ and ‘r’ denote the blue-arm (echelle order 102) and red-arm (echelle orders 90 and 83) exposures; calibration lamp exposures were taken immediately after each science exposure; the pixel sizes close to the Fe II lines, where the S/N has been computed, are 25 mÅ ($\lambda 1608$), 30 mÅ ($\lambda 2382$), and 27 mÅ ($\lambda 2600$).

perature can induce color effects in the spectra since they act differently on the different cross dispersers.

To control possible systematics in radial velocities, the thermal and pressure stabilities were monitored. Variations of the ambient temperature during science exposures (the difference ΔT between the beginning and the end) were always less than 0.1 K. This is also the maximum variation occurring between the science exposure and the calibration lamp. The pressure variation ΔP reached 0.6 mbar in one case (No. 4, Table 1), in all other cases the variations of ΔP did not exceed 0.3 mbar. The estimations of Kaufer et al. (2004) are of 50 m s^{−1} for $\Delta T = 0.3$ K and $\Delta P = 1$ mbar, so the observed differences should not affect significantly the radial velocities.

From the blue frame we used only order 102, and from the red — orders 90 and 83 (Col. 5), where Fe II lines with, respectively, $\lambda = 1608$, 2382 and 2600 Å are observed. The selected lines are located close to the central regions of the corresponding echelle orders. This minimizes possible distortions of the line profiles caused by the decreasing spectral sensitivity at the edges of echelle orders. The signal-to-noise ratios (S/N) per pixel (25 mÅ, 30 mÅ and 27 mÅ at the positions of $\lambda 1608$, $\lambda 2382$ and $\lambda 2600$, respec-

tively) for the individual exposures and individual orders are listed in Col. 6. Cols. 2, 3 and 4 give, respectively, the date of observation, the beginning of the exposure, and the total exposure time.

The spectra were reduced using the UVES context within the ESO MIDAS data reduction software. Master flat-field and master bias frames were obtained by computing the median of five flat-field and bias frames taken in the afternoon. The master bias was subtracted from each science frame; subsequently the background was subtracted by fitting a two-dimensional spline to points in the inter-order region, where the background was estimated as the median number of counts over a box 51 pixels wide in the dispersion direction and 5 pixels wide in the cross-dispersion direction. The background subtracted science frame was divided pixel-by-pixel by the normalized master flat-field. The spectrum was extracted using an average extraction and an optimal extraction. The S/N ratio proved to be higher in the average extraction, therefore this was used for the analysis. The wavelength calibration was derived from the spectrum of a ThAr hollow cathode lamp. We used the Los Alamos table of ThAr lines (Palmer & Engleman 1983; de Cuyper & Hensberge 1988) and the 1D option, by which a 4th order polynomial is fit to the measured positions of arc lines in each echelle order. The wavelength calibration was applied to the extracted science spectrum both on a pixel by pixel basis, and rebinning the extracted spectrum to a constant wavelength step. We did not observe any systematic shift in the line centroids introduced by the rebinning, therefore we used the rebinned spectra, which can be readily co-added. We kept a very small tolerance in the fitting in order to reject several faint lines with lower accuracy (about 150 m s^{−1}) still preserving somewhat 20 lines for each order, normally strong lines with about 15 m s^{−1} accuracy. Finally, as a cross-check, we performed an independent reduction of the spectra using a 2D wavelength calibration, by which a 2D polynomial dispersion relation of the form $f(m, \lambda)$, where m is the absolute order number and λ is the wavelength, is fitted to the entire echellogram of the ThAr lamp (Lopez et al. 2005). The residuals of the calibrations in both approaches were rather small corresponding to the rms errors of the wavelength scale calibration of about 20 m s^{−1}. The observed wavelength scale of each spectrum was transformed into vacuum, heliocentric wavelength scale (Edlén 1966). The resulting spectral resolution as measured from the ThAr emission lines was $FWHM \simeq 3.95$ km s^{−1} in the blue ($\lambda \sim 4500$ Å) and $\simeq 3.75$ km s^{−1} in the red ($\lambda \sim 7000$ Å). Thus, the resolution of these new spectra is significantly higher than in the previous observations (6 and 5.4 km s^{−1} respectively, see Paper I).

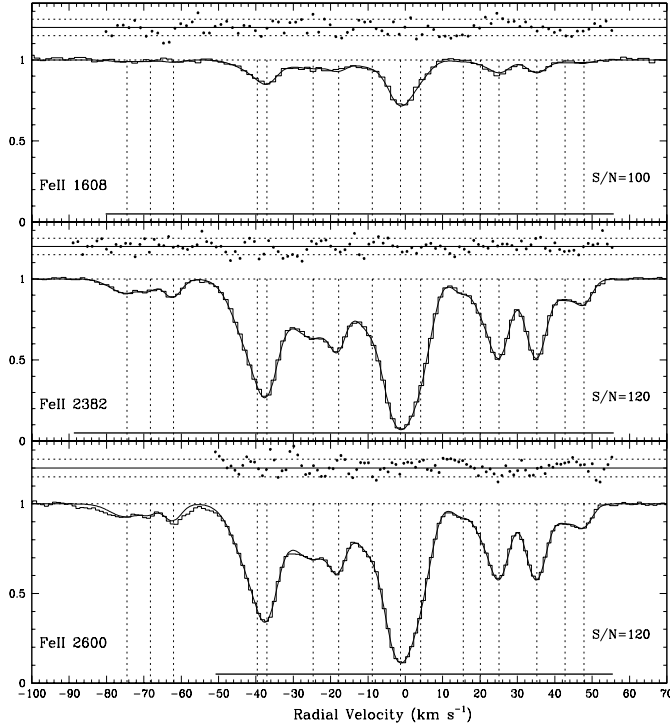


Fig. 1. Combined absorption-line spectra of Fe II associated with the $z = 1.84$ damped Ly α system towards Q 1101–264 (normalized intensities are shown by histograms). The zero radial velocity is fixed at $z_{\text{abs}} = 1.838911$. The synthetic profiles are over-plotted by the smooth curves. The normalized residuals, $(\mathcal{F}_i^{\text{cal}} - \mathcal{F}_i^{\text{obs}})/\sigma_i$, are shown by dots (horizontal dotted lines restrict the 1σ errors). The dotted vertical lines mark positions of the sub-components. Bold horizontal lines mark pixels included in the optimization procedure. The ranges at $v < -50 \text{ km s}^{-1}$ and at $v \simeq -30 \text{ km s}^{-1}$ in the Fe II $\lambda 2600$ profile are blended with weak telluric lines. The normalized $\chi^2_{\nu} = 0.901$ ($\nu = 257$).

3. Estimate of $\Delta\alpha/\alpha$

The spectroscopic measurability of $\Delta\alpha/\alpha$ is based on the fact that the energy of each line transition depends individually on a change in α (e.g., Webb et al. 1999). It means that the relative change of the frequency ω_0 due to varying α is proportional to the so-called sensitivity coefficient $Q = q/\omega_0$ (Paper I). The q -values for the resonance UV transitions in Fe II are calculated by Dzuba et al. (2002). The corresponding sensitivity coefficients are listed in Table 5 in Paper II. The rest frame wavelengths for some Fe II transitions have been re-measured recently with higher accuracy by Aldenius et al. (2006). For our present work we need two of them: $2382.7641 \pm 0.0001 \text{ \AA}$, and $2600.1722 \pm 0.0001 \text{ \AA}$. The line from the 8th UV multiplet $1608.45080 \pm 0.00008 \text{ \AA}$ in Table 5 is registered to

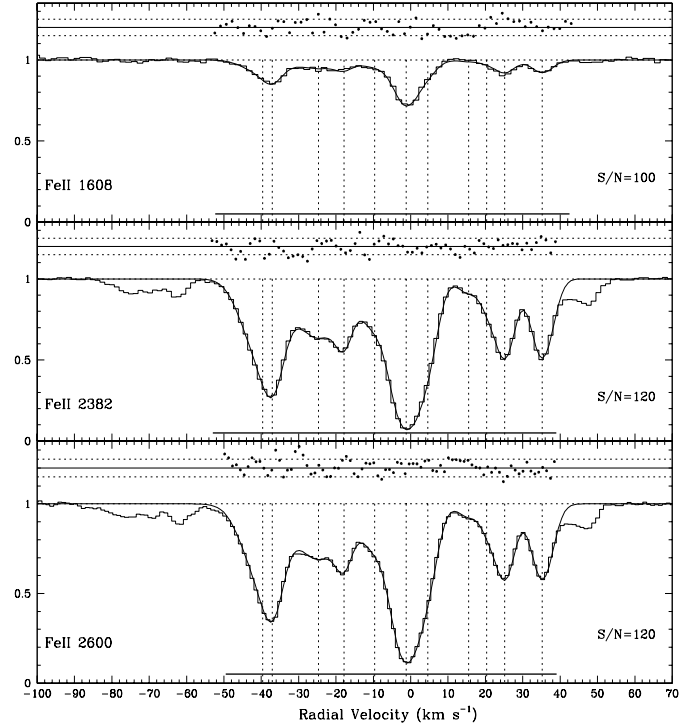


Fig. 2. Same as Fig. 1 but for the 11-component model fitted to the central part of the Fe II lines. The normalized $\chi^2_{\nu} = 0.720$ ($\nu = 188$).

the calibration scale defined in Norlén (1973), whereas the lines $\lambda 2382$ and $\lambda 2600$ from Aldenius et al. are calibrated in the scale of Whaling et al. (1995). The two scales differ by a factor of about 7×10^{-8} in frequency space. Thus, a corrected wavelength of the $\lambda 1608$ line is 1608.45069 \AA . Other atomic data are taken as they are in Table 5.

The value of $\Delta\alpha/\alpha$ itself depends on a proper interpretation of measured relative radial velocity shifts, Δv , between lines with different sensitivity coefficients, ΔQ . It can be shown that in linear approximation ($|\Delta\alpha/\alpha| \ll 1$) these quantities are related as (Paper II):

$$\frac{\Delta\alpha}{\alpha} = \frac{(v_2 - v_1)}{2c(Q_1 - Q_2)} = \frac{\Delta v}{2c\Delta Q}. \quad (1)$$

Here index ‘1’ is assigned to the line $\lambda 1608$, while index ‘2’ marks one of the other Fe II lines ($\lambda 2382$ or $\lambda 2600$).

It is important that ΔQ must be large enough to provide smaller uncertainty in $\Delta\alpha/\alpha$. With $Q_1 = -0.021$ and $Q_2 = 0.035$ for both $\lambda 2382$ and $\lambda 2600$ lines, we have $\Delta Q = -0.056$. Note that $|\Delta Q| = 0.056$ is almost two times larger than $|\Delta Q| \simeq 0.03$ which is used in the standard MM method when Mg II $\lambda \lambda 2796, 2803$ and Fe II $\lambda \lambda 2344, 2374, 2382, 2586, 2600$ transitions are compared¹.

¹ For Mg II, $Q_{2796} = 0.0059$, and $Q_{2803} = 0.0034$. For Fe II, $Q_{2344} = 0.028$, $Q_{2374} = 0.038$, and $Q_{2586} = 0.039$.

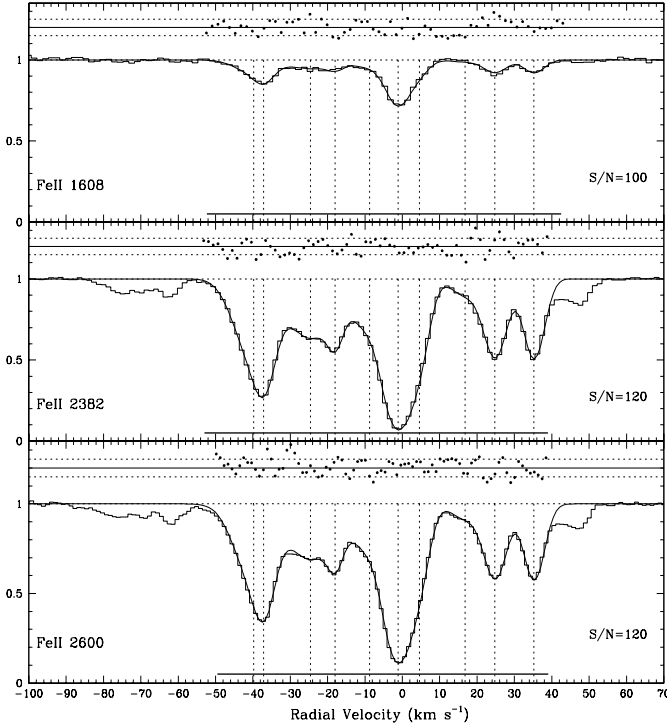


Fig. 3. Same as Fig. 2 but for the 10-component model. The normalized $\chi^2_\nu = 0.871$ ($\nu = 191$).

It is also important that the Fe II transitions at $\lambda 1608$ and $\lambda\lambda 2382, 2600$ used in the present study have sensitivity coefficients of different signs which helps to distinguish the influence of hidden blends on the line position measurements (Levshakov & D’Odorico 1995).

The individual vacuum-barycentric spectra were re-sampled to equidistant wavelength grids using smallest pixel sizes in the blue and red exposures and applying linear interpolation. The resulting normalized and co-added spectra from 9 exposures (Table 1) are shown in Fig. 1. A weighted mean signal-to-noise ratio per pixel of $S/N = 100$ and 120 was achieved in the final spectrum at $\lambda \sim 4566$ Å and $\lambda \sim 6765, 7382$ Å, respectively. Two independent data reduction procedures resulted in almost identical co-added spectra. In contrast to the archive data used in Paper I which we failed to fit self-consistently, this time we found a good fit of Fe II profiles to a model, the normalized χ^2 per degree of freedom equals $\chi^2_\nu = 0.901$ ($\nu = 257$). The computational procedure was the same as in Paper II. The optimal solution was found for the 16-component model shown in Fig. 1 by the smooth curves (the positions of the sub-components are marked by dotted lines). The model parameters are given in Table 2. Since the Q values for $\lambda 2382$ and $\lambda 2600$ are equal, their relative velocity shift characterizes the goodness of wavelength calibrations of the echelle orders 90 and 83. The revealed velocity shift of 20 m s^{-1} is comparable with the uncertainty range esti-

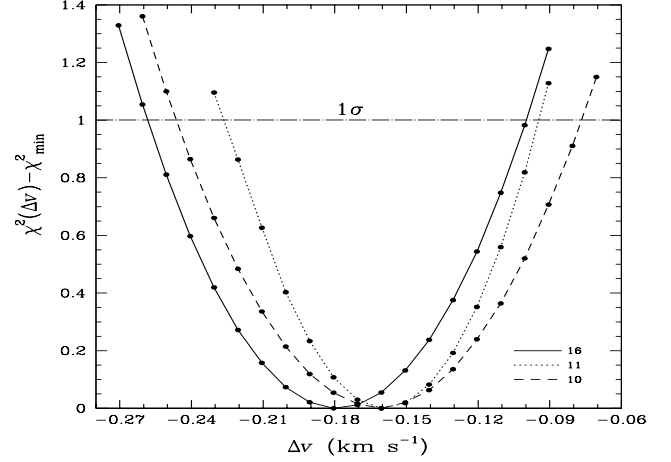


Fig. 4. χ^2 as a function of the velocity difference Δv between the Fe II $\lambda 1608$ and $\lambda\lambda 2382, 2600$ lines for the 16-, 11-, and 10-component models which are shown, respectively, in Figs. 1, 2, and 3. The corresponding χ^2_{\min} values are equal to 231.631, 135.314, and 166.397. The minima of the curves give the most probable values of $\Delta\alpha/\alpha$ (see eq.[1]): 5.4 ppm (the 16-component model) and 4.8 ppm (the 11- and 10-component models). The 1σ confidence level is determined by $\Delta\chi^2 = 1$ which gives $\sigma_{\Delta v} = 0.080 \text{ km s}^{-1}$, 0.065 km s^{-1} , and 0.085 km s^{-1} or $\sigma_{\Delta\alpha/\alpha} = 2.4 \text{ ppm}$, 1.9 ppm , and 2.5 ppm for the 16-, 11-, and 10-component models, respectively.

mated from the ThAr lines. So, in what follows we consider $\lambda 2382$ and $\lambda 2600$ as having the same radial velocity, and calculate Δv between this velocity and that of the line $\lambda 1608$.

To demonstrate that our result is not sensitive to the number of subcomponents, we have analyzed different models. The 16-component model is chosen as one which covers the whole Fe II profile in the range from -90 km s^{-1} to 55 km s^{-1} (Fig. 1) and provides $\chi^2_\nu \lesssim 1$ with minimum number of components. The other models are shown in Figs. 2 and 3 with the corresponding parameters listed in Table 2. The 11-component model in Fig. 2 ignores the weak absorption in the wings of the Fe II lines at $-90 \text{ km s}^{-1} \lesssim v \lesssim -55 \text{ km s}^{-1}$ and $40 \text{ km s}^{-1} \lesssim v \lesssim 55 \text{ km s}^{-1}$. In the model shown in Fig. 3 the number of components is reduced to 10 which is found to be the lower limit since models with 9 components cannot be fitted adequately to the Fe II lines in the range $-55 \text{ km s}^{-1} \lesssim v \lesssim 40 \text{ km s}^{-1}$ with χ^2_ν less than 3. We note that all of the analyzed models show similar radial velocity shifts between the $\lambda 1608$ and $\lambda\lambda 2383/2600$ lines. The comparison between the theoretical and observed Fe II profiles was quantified by the χ^2 function (defined by eq.[2] in Paper II). To find the most probable value of Δv , we fit the

absorption lines with a fixed Δv , changing Δv in the interval from -270 m s^{-1} to -90 m s^{-1} in steps of 10 m s^{-1} (see Fig. 4). For each Δv , the strengths of the sub-components, their broadening parameters and relative velocity positions were allowed to vary in order to optimize the fit and thus minimize χ^2 . The χ^2 curve as a function of Δv in the vicinity of the global minimum must be smooth and have a parabola-like shape. The most probable value of Δv corresponds to the minimum of χ^2 . In our case it is -180 m s^{-1} for the 16-component model. The 1σ confidence interval to this value is given by $\Delta\chi^2 = \chi^2 - \chi^2_{\min} = 1$ (e.g., Press et al. 1992), which is shown by the horizontal dashed line in Fig. 4. It is seen from the figure that the 1σ errors are equal to 80 m s^{-1} , 65 m s^{-1} , and 85 m s^{-1} for the models in question. Adding quadratically the wavelength scale calibration error between the blue and red arms of 30 m s^{-1} and using (1), one can easily obtain $\Delta\alpha/\alpha = 5.4 \pm 2.5 \text{ ppm}$ for the main 16-component model.

4. Possible systematics

We have specifically investigated those effects which might introduce a non-zero difference between the blue and the red lines and thus simulate a $\Delta\alpha/\alpha$ variation at the ppm level. In addition to the systematics discussed in Sect. 2, the following factors should be taken into account.

Systematic shift between the blue and red arms. Different velocity offsets may occur in the blue and red frames causing an artificial Doppler shift between the $\lambda 1608$ and $\lambda 2382/2600$ lines. To probe this effect we used the same procedure as for the QSO exposures and calibrated in wavelength the spectra of the ThAr arcs. For the blue and red frames we selected well-exposed ThAr emissions which bracket the positions of the Fe II $\lambda 1608$ and $\lambda 2382/2600$ lines. The calibrated ThAr spectra do not show the rms errors larger than 20 m s^{-1} . In Fig. 3, an example of the residuals (open circles) between the laboratory and fitted ThAr wavelengths for the 4th exposure is shown. The total number of ThAr lines used to calculate the rms error in the echelle order is indicated on each panel, whereas only the ThAr lines close to the observed positions of the Fe II lines of interest are depicted. A conservative shift between the blue and red arms of 30 m s^{-1} can be obtained if the rms error of 20 m s^{-1} is taken for each arm.

Centering the target onto the slit. Radial velocity shifts induced by different changes of isophote onto the slit are not chromatic, i.e. the shifts are the same in the blue and red UVES arms. The fact that we have re-centered the object in the different nights and also before and after passage to the meridian assure that the effect was different from one exposure to the other, and, hence, averaged out in the mean spectrum. Besides, tracking movements act in smoothing the isophote onto the slit. We note that in

our previous results on HE 0515–4414 (Paper II) we also used Fe II lines falling in both UVES arms without showing evidence of shifts.

Isotopic shifts. Using the mass shift constants k_{MS} calculated by Kozlov et al. (2004), we estimated the uncertainty of $\Delta\alpha/\alpha \simeq 0.77 \text{ ppm}$ caused by unknown isotope abundances (Paper I) which is equivalent to the uncertainty of about 20 m s^{-1} .

Unresolved components. The normalized residuals, $(\mathcal{F}_i^{\text{cal}} - \mathcal{F}_i^{\text{obs}})/\sigma_i$, in Figs. 1, 2, and 3 do not show series which could suggest unresolved Fe II components.

Possible blends. The $\lambda 1608$ and $\lambda 2382$ lines lie in the spectral regions free from telluric absorptions. No metal absorption lines from other systems which could blend with these iron lines were found as well. Weak night sky absorptions affect the $\lambda 2600$ profile at $v = -30 \text{ km s}^{-1}$ and in the range $v < -50 \text{ km s}^{-1}$ which was not included in the fitting of this line. Since both the $\lambda 2382$ and $\lambda 2600$ lines are considered as having the same radial velocity and the line $\lambda 2382$ is clean, this contamination of $\lambda 2600$ does not influence the final value of $\Delta\alpha/\alpha$.

5. Conclusions

We have re-observed the quasar Q 1101–264 with spectral resolution $FWHM \sim 3.8 \text{ km s}^{-1}$ and re-analyzed the Fe II profiles associated with the $z = 1.84$ damped Ly α system. The data represent one of very few spectra of QSOs obtained with this high resolution and $S/N \gtrsim 100$. The newly obtained value of the relative radial velocity shift $\Delta v = -180 \pm 85 \text{ m s}^{-1}$ between the $\lambda 1608$ and $\lambda 2382, 2600$ lines represents a factor of 1.5 improvement with respect to lower resolution archive data ($FWHM \sim 6 \text{ km s}^{-1}$, Paper I). Admittedly, there might be further hidden systematic effects which would challenge the interpretation as due to variation of α . If real, it would correspond to $\Delta\alpha/\alpha = 5.4 \pm 2.5 \text{ ppm}$. Thus, the highest spectral resolution achievable on QSO spectra at 8–10 m telescopes is proved to significantly contribute to higher accuracy in the $\Delta\alpha/\alpha$ measurement.

We note that averaging the 8 systems in the redshift interval $1.5 < z < 2.0$ of Chand et al. (2004) one obtains $\Delta\alpha/\alpha = 2.4 \pm 1.2 \text{ ppm}$. On the other hand, Murphy et al. (2003) results averaged over the same redshift interval (16 systems) give $\Delta\alpha/\alpha = -5.4 \pm 4.5 \text{ ppm}$. Whereas the Chand et al. and our values are consistent within the 1σ confidence interval, the value of Murphy et al. is significantly different.

Up to now, we have obtained high precision measurements of the $\Delta\alpha/\alpha$ with the SIDAM method at two redshifts, $z = 1.15$ and $z = 1.84$, only. Of course, to probe the true redshift evolution of α many more measurements are needed. It should be understood, however, that such measurements are extremely hard to perform since they

Table 2. SIDAM analysis: positions, v (in km s^{-1}), of the Fe II sub-components, the line broadening parameters, b (in km s^{-1}), and the column densities N_{12} (in the units of 10^{12} cm^{-2}) for the 16-, 11-, and 10-component models shown in Figs. 1, 2, and 3 (the corresponding uncertainties of the fitting parameters are less than 5%). The v values are referred to the $\lambda 1608 \text{ \AA}$ line, whereas the positions of the $\lambda 2382$ and $\lambda 2600 \text{ \AA}$ lines are shifted at $v' = v + \Delta v$ with the optimal values of Δv given in Fig. 4.

No.	v 16-component model	b 16-component model	N_{12} 16-component model	v 11-component model	b 11-component model	N_{12} 11-component model	v 10-component model	b 10-component model	N_{12} 10-component model
1	-74.494	5.36	0.48						
2	-68.198	1.59	0.11						
3	-62.067	2.42	0.34						
4	-39.630	6.39	3.92	-39.643	6.30	3.95	-39.661	6.30	3.91
5	-37.029	2.85	2.36	-37.018	2.79	2.30	-37.046	2.82	2.33
6	-24.643	7.02	2.90	-24.650	7.14	2.95	-24.497	7.30	3.02
7	-17.879	2.05	0.99	-17.837	2.11	1.03	-17.902	1.86	0.90
8	-8.875	5.69	2.02	-9.677	4.67	1.58	-8.667	6.13	2.11
9	-1.279	3.60	9.56	-1.171	3.88	10.60	-1.072	3.76	10.15
10	4.085	3.31	2.67	4.607	3.03	2.00	4.639	2.92	2.01
11	15.493	2.77	0.29	15.504	3.02	0.31	16.905	4.47	0.47
12	20.110	1.18	0.28	20.352	1.50	0.34			
13	25.089	3.03	2.31	25.145	2.89	2.23	24.873	3.45	2.43
14	35.192	2.95	2.25	35.232	3.10	2.31	35.288	2.95	2.27
15	42.746	2.36	0.33						
16	47.827	2.31	0.48						

require spectral data of highest quality which can be obtained for the brightest QSOs only. In spite of the fact that many giant telescopes were put into operation in the last decades, the unique simultaneous wavelength coverage $3000 \text{ \AA} < \lambda < 10000 \text{ \AA}$ of UVES makes it the only instrument suitable for this work. Thus, the progress in our understanding the evolution of $\Delta\alpha/\alpha$ and, hence, of dark energy is expected to be ‘slow-rolling’ until more powerful Extremely Large Telescopes will come into operation.

Acknowledgements. S.A.L. and I.I.A. gratefully acknowledge the hospitality of Hamburger Sternwarte. This research has been supported by the RFBR grant No. 06-02-16489, by the Federal Agency for Science and Innovations grant NSh 9879.2006.2, and by the DFG project RE 353/48-1. P.M. thanks Ville de Paris for an international fellowship. S.L. was partly supported by the Chilean Centro de Astrofísica FONDAP No. 15010003, and by FONDECYT grant N°1060823.

References

- Aldenius, M., Johansson, S., & Murphy, M. T., 2006, MNRAS, 370, 444
- Avelino, P. P., Martins, C. J. A. P., Nunes, N. J., & Olive, K. A. 2006, Phys. Rev. D, 74, 083508
- Cingöz, A., Lapierre, A., Nguyen, A.-T. et al. 2007, Phys. Rev. Lett., 98, 040801
- Copeland, E. J., Sami, M., & Tsujikawa, S. 2006, Int. J. Mod. Phys., D15, 1753
- Chand, H., Srianand, R., Petitjean, P., et al. 2006, A&A, 451, 45
- Chand, H., Srianand, R., Petitjean, P., & Aracil, B. 2004, A&A, 417, 853
- de Cuyper, J.-P., & Hensberge, H. 1988, A&AS, 129, 409
- Dvali, G., Gabadadze, G., & Porrati, M. 2000, Phys. Lett. B, 485, 208
- Dzuba, V. A., Flambaum, V. V., Kozlov, M. G., & Marchenko, M. V. 2002, Phys. Rev. A, 66, 022501
- Edlén, B. 1966, Metrologia, 2, 71
- Fujii, Y., & Maeda, K. 2003, *The scalar-tensor theory of gravitation* (Cambridge Univ. Press: Cambridge)
- Gould, C. R., Sharapov E. I., & Lamoreaux, S. K., 2006, Phys. Rev. C, 74, 024607
- Hao, H., Stanek, K. Z., Dobrzycki, A. et al. 2006, ApJ, submit. (astro-ph/0612409)
- Kaufer, A., D’Odorico, S., & Kaper, L. 2004, UV-Visual Echelle Spectrograph. User Manual (<http://www.eso.org/instruments/uves/userman/>), p. 40
- Kozlov, M. G., Korol, V. A., Berengut, J. C., Dzuba, V. A., & Flambaum, V. V. 2004, Phys. Rev. A, 70, 062108
- Liddle, A. R., & Lyth, D. H. 2000, *Cosmological inflation and large-scale structure* (Cambridge Univ. Press: Cambridge)
- Levshakov, S. A., Centurión, M., Molaro, P., et al. 2006, A&A, 449, 879 [Paper II]
- Levshakov, S. A., Centurión, M., Molaro, P., & D’Odorico, S. 2005, A&A, 434, 827 [Paper I]
- Levshakov, S. A. 2004, in *Astrophysics, Clocks and Fundamental Constants*, eds. S. G. Karshenboim and E. Peik (Springer-Verlag: Berlin, Heidelberg), p.151
- Levshakov, S. A., & Kegel, W. H. 1997, MNRAS, 288, 787
- Levshakov, S. A., Kegel, W. H., & Mazetz, I. E. 1997, MNRAS, 288, 802
- Levshakov, S. A., & D’Odorico, S. 1995, in QSO Absorption Lines, ed. G. Meylan, p.202
- Lopez, S., Reimers, D., Gregg, M., et al., 2005, ApJ, 626, 767
- Murphy, M. T., Flambaum, V. V., Webb, J. K., et al. 2004, in *Astrophysics, Clocks and Fundamental Constants*, eds. S. G. Karshenboim and E. Peik (Springer-Verlag: Berlin, Heidelberg), p.131

- Murphy, M. T., Webb, J. K., & Flambaum, V. V. 2003, MNRAS, 345, 609
- Norlén, G. 1973, Phys. Scr., 8, 249
- Palmer, B. A., & Engleman, R., Jr. 1983, *Atlas of the Thorium Spectrum*, LA-9615
- Porciani, C., Viel, M., & Lilly, S. J. 2007, ApJ, in press (astro-ph/0701153)
- Press, W. H., Teukolsky, S. A., & Vetterling, W. T., & Flannery, B. P. 1992, *Numerical Recipes in C* (Cambridge Uni. Press: Cambridge)
- Quast, R., Reimers, D., & Levshakov, S. A. 2004, A&A, 415, L7
- Whaling, W., Anderson, W. H. C., Carle, M. T., Brault, J. W., & Zarem, H. 1995, J. Quant. Spectrosc. Radiat. Transfer, 53, 1
- Webb, J. K., Flambaum, V. V., Churchill, C. W., Drinkwater, M. J., & Barrow, J. D. 1999, Phys. Rev. Lett., 82, 884

List of Objects

- ‘Q 1101–264’ on page 1
- ‘Q 1101–264’ on page 1
- ‘Q 1101–264’ on page 1
- ‘HE 0515–4414’ on page 2
- ‘Q 1101–264’ on page 2
- ‘Q 1101–264’ on page 2
- ‘Q 1101–264’ on page 3
- ‘Q 1101–264’ on page 4
- ‘Q 1101–264’ on page 6

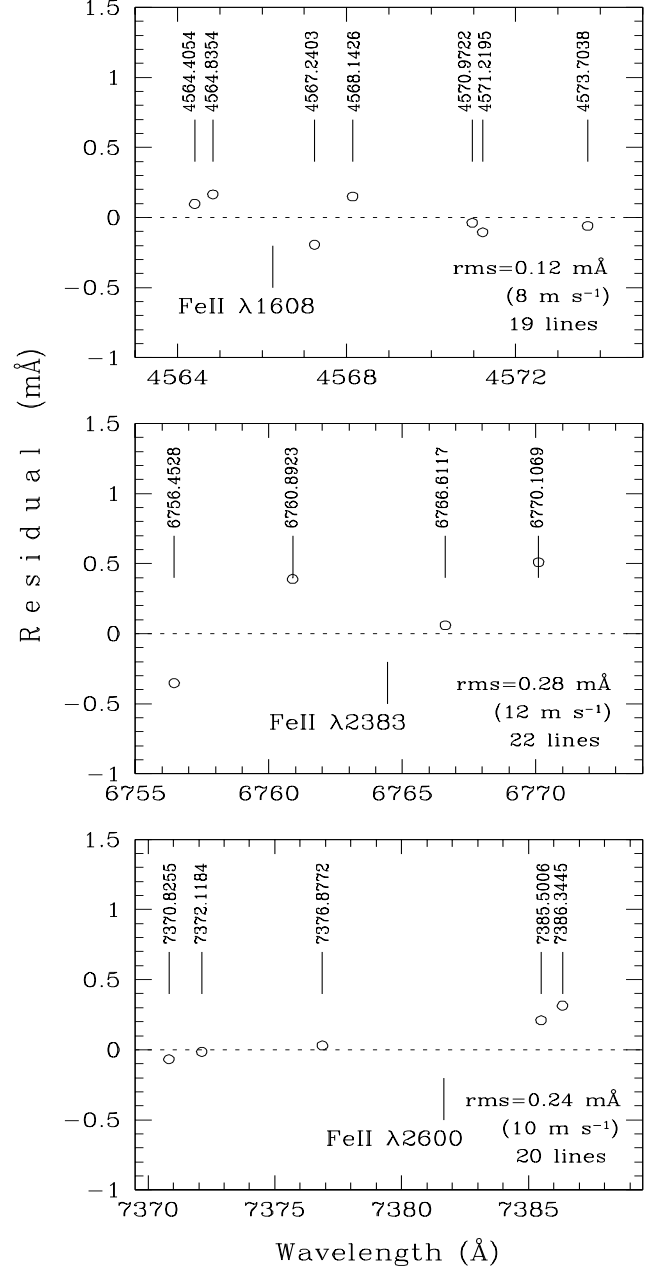


Fig. 5. An example of the residuals (open circles) between the laboratory and fitted ThAr wavelengths for the 4th exposure. The total number of the well-defined ThAr lines used to calculate the rms error in the echelle order is indicated on each panel, whereas only the ThAr lines close to the observed positions (marked by vertical bars) of the Fe II lines of interest are depicted.